Liquid Crystals

ISSN: (Print) (Online) Journal homepage: www.tandfonline.com/journals/tlct20

A ferroelectric nematic liquid crystal vitrified at room temperature

A. Adaka, P. Guragain, K. Perera, P. Nepal, B. Almatani, S. Sprunt, J. Gleeson, R. J. Twieg & A. Jákli

To cite this article: A. Adaka, P. Guragain, K. Perera, P. Nepal, B. Almatani, S. Sprunt, J. Gleeson, R. J. Twieg & A. Jákli (28 Apr 2024): A ferroelectric nematic liquid crystal vitrified at room temperature, Liquid Crystals, DOI: 10.1080/02678292.2024.2345214

To link to this article: https://doi.org/10.1080/02678292.2024.2345214

LIQUID CRYSTALS
https://doi.org/10.1080/02678292.2024.2345214

A ferroelectric nematic liquid crystal vitrified at room temperature

A. Adaka[a,b], P. Guragain[c], K. Perera[a,d], P. Nepal[c], B. Almatani[d], S. Sprunt[d], J. Gleeson[d], R. J. Twieg[c] and A. Jákli[a,b,d]

[a]Advanced Materials and Liquid Crystal Institute, Kent State University, Kent, OH, USA; [b]Materials Science Graduate Program, Kent State University, Kent, OH, USA; [c]Department of Chemistry and Biochemistry, Kent State University, Kent, OH, USA; [d]Department of Physics, Kent State University, Kent, OH, USA

ABSTRACT

Most of the current highly polar rod-shaped molecules that form ferroelectric nematic (N_F) phase do so only at elevated temperatures and multicomponent mixtures are generally needed to obtain a broad and room temperature range N_F phase. In this work, we describe the synthesis, phase characterisation and measurement of various physical properties of a new ferroelectric nematic compound 4-[(4-nitrophenoxy)carbonyl]phenyl 2-isopropoxy-4-methoxybenzoate (RT11165). The molecular structure of RT11165 with a 2-isopropoxy group differs only by a substitution of the 2-methoxy group found in the prototype ferroelectric nematic material 4-[(4-nitrophenoxy)carbonyl]phenyl 2,4-dimethoxybenzoate (RM734). This small structure change produces a rather dramatic change in phase behaviour leading to an N_F phase from 63°C down to room temperature. Below about 45°C the rotational viscosity of RT11165 increases critically and the temperature dependence indicates a glass transition at ~19°C. The transparent and polar glassy state of RT11165, which should be also piezoelectric, is a good candidate for energy storage, piezoecatalysis, data storage and other applications.

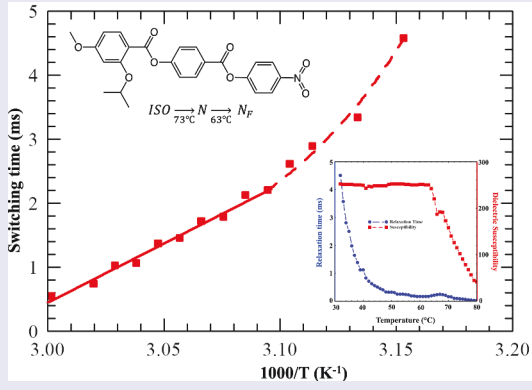

ARTICLE HISTORY
Received 18 March 2024
Accepted 16 April 2024

KEYWORDS
Liquid crystal; polarisation; room temperature ferroelectric nematic; Polar glassy liquid crystal

1. Introduction

Most contemporary liquid crystal-based flat panel TVs [1] use nematic liquid crystals that are 3D anisotropic fluids in which the optical properties can be reversibly switched without breaking the long-range orientational order. Since the discovery of liquid crystals in 1888 [2], in addition to the uniaxial non-polar nematic liquid crystals used in displays, there have been several other nematic liquid crystal phases predicted and experimentally observed, such as the chiral nematic (N*) [2], biaxial nematic (N_b) [3] bent-core nematic (N_{bc}) [4], twist-bend [5–9] and ferroelectric nematic (N_F) [10–15] phases. The N_F phase that has been experimentally observed only a few years ago, requires large $(|\vec{\mu}|) > 9Debye)$ molecular dipoles that spontaneously align parallel to each other. This results in a macroscopic polarisation $\vec{P} = \frac{\langle\vec{\mu}\rangle\rho N_A}{M} = \frac{S\vec{\mu}\rho N_A}{M}$, where ρ is the mass density, $N_A \approx 6 \cdot 10^{23}$ is the Avogadro number, M is the molar mass and $S \leq 1$ is the dipolar order parameter. Assuming perfect dipolar order $(S = 1)$ and using typical values, such as $\mu = 10Debye \approx 3.3 \cdot 10^{-29}Cm$, $\rho \approx 1.3 \cdot 10^3 kg/m^3$, $M \approx 0.4kg$, we find that $P = 6.4 \cdot 10^{-2}C/m^2$ is in accordance with experimental observations [13,15,16].

Most of the currently known highly polar rod-shaped molecules possess an N_F phase only at elevated

CONTACT A. Jákli ajakli@kent.edu
Supplemental data for this article can be accessed online at https://doi.org/10.1080/02678292.2024.2345214.

temperatures, and multicomponent mixtures [17–20] are generally needed to provide a broad and room temperature range N_F phase. Only a few single component materials show an N_F phase below or at room temperature [21–23].

In this work, we describe the design, synthesis, and characterisation of various physical properties of a new ferroelectric nematic compound 4-[(4-nitrophenoxy)carbonyl]phenyl 2-isopropoxy-4-methoxybenzoate (RT11165). The molecular structure of RT11165 differs from the prototypical ferroelectric nematic compound 4-[(4-nitrophenoxy)carbonyl]phenyl 2,4-dimethoxybenzoate (RM734) [12,24] only by a replacement of the 2-methoxy group with a 2-isopropoxy group. We will show that this small structural change [25–27] produces a rather dramatic change in the N_F range permitting ferroelectric switching at room temperature upon application of a DC voltage while the material flow is hindered.

2. Material and methods

The goal to identify a substance with a particular physical property optimised at room temperature is certainly not unique to the field of liquid crystals. A specific earlier relevant example involved the need to produce an organic photorefractive material that functioned at room temperature. In that case one solution involved the design of a composition containing a glass forming chromophore by modification of a substituent of a methylene-dihydropyridine molecule [28]. The same sort of strategy has been applied here by the substitution of a methoxy group in RM734 that has an I – 187°C – N – 133 °C – N_F phase sequence, with an isopropoxy group in RT11165 (4-[(4-nitrophenoxy) carbonyl] phenyl 2-isopropoxy-4-methoxybenzoate that leads to an I – 73°C – 63°C – N_F phase sequence. This structure, which involves a change from a primary to a secondary substituent, is not unique. For example, derivatives of RM734, which have such a substructure made from chiral 2-butanol and 2-octanol, have been described [29]. The molecular structure of RT11165 is shown at the top of Figure 1. The steps of chemical synthesis, chemical characterisation, and the DSC scans in the first and second heating-cooling cycles of RT11165 are provided in the Supporting Information (SI).

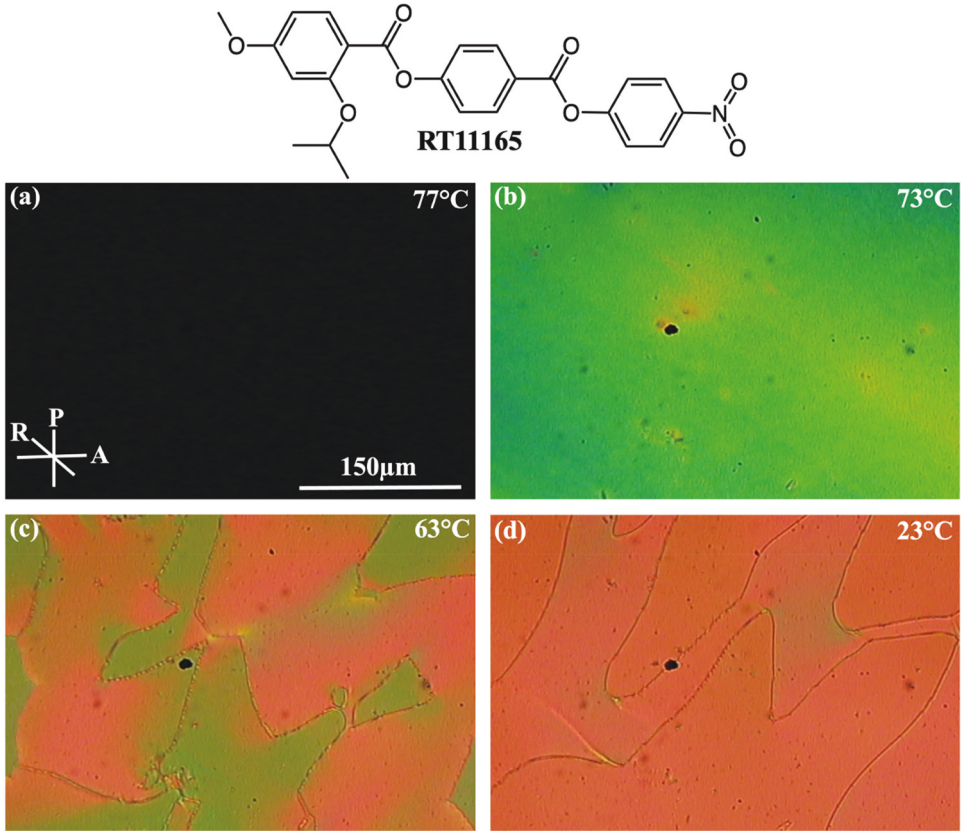

Figure 1. (Colour online) Molecular structure of RT11165 (top) and polarising optical microscopy (POM) images at different temperatures of RT11165 during cooling at 1°C/min rate. (a) Isotropic phase; (b) Nematic phase; (c) Ferroelectric nematic after the transition from nematic; (d) Ferroelectric nematic phase at room temperature.

Polarised optical microscopy (POM) studies were carried out on a $L = 11.3\mu m$ thick sandwich cell placed in an Instec HS200 heat stage equipped with an STC200D controller, using an Olympus B × 60 microscope. The substrates of the RT11165 sample were treated for uniform planar alignment using a polyimide PI2555 coating and rubbed unidirectionally parallel to each other. Beneath the PI2555 coating the bottom plate has two $3mm$ wide conducting indium tin oxide (ITO) strips separated by a $0.5mm$ gap, while the top plate has no ITO layer. The cells were assembled using NOA68 glue mixed with 10 µm spacers to achieve uniform thickness. An HP 33120A 15 MHz function/arbitrary waveform generator was used to generate voltage and amplified by a Model BOP 500 M 50X Kepco Bipolar Operational amplifier to obtain the desired applied AC voltages.

Ferroelectric polarisation measurements were carried out by applying 35–70 Hz triangular waveform voltages between the in-plane electrodes. To measure the polarisation current $I_P = \dot{Q}_P$, a Princeton Applied Research Model 181 current preamplifier with sensitivity $\frac{I}{V} = 10^{-4}$ was used. The value of the ferroelectric polarisation P was calculated from the area $Q_P = \int \dot{Q}_P dt$ of the polarisation current peak $\dot{Q}_P$ measured between the in-plane electrodes, assuming the polarisation charge accumulated at the in-plane electrodes is $Q_P = P \cdot A$ [13], where $A = d \times l$ is the cross sectional area normal to the polarisation vector with l being the length of the ITO strips and d is the film thickness. In our case $A = 8.5mm \times 11.3\mu m = 9.605 \times 10^{-8} m^2$.

The frequency-dependent complex dielectric permittivity $\varepsilon(\omega) = \varepsilon'(\omega) - i\varepsilon''(\omega)$ was measured between 22°C and 77°C with an HP 4284A LCR metre by applying 30 mV amplitude sinusoidal AC voltage in the frequency range of 100 Hz − 1 MHz between patterned ITO coated glass plates of a sandwich cell with planar alignment (cell gap: $d = 12.2\mu m$, cell area: $A = 1cm^2$).

Electro-optical measurements were carried out using cells of various thickness between $3.5\mu m - 10.7\mu m$ under square wave AC voltages applied by a HP 33120A 15 MHz function/arbitrary waveform generator and DC Voltage using a HP Harrison 6110A DC power supply to study the switching of the samples from $25°C$ to $65°C$.

Switching times were determined at various temperatures from the time dependences of the polarisation current under $450V$, $40Hz$ rectangular wave voltages applied across the 0.5 mm gap between in-plane electrodes. The rise time τ (the time for the polarisation current to reach 90% of its maximum) as found by Chen et al. [13] is proportional to the polarisation reversal time Δt obtained from the full width at half maxima (FWHM) of the polarisation current peak (see inset to Figure 3).

3. Results and discussion

POM images of a $11.5\mu m$ thick film with antiparallel rubbed planar alignment coating at various temperatures during cooling at $2°C/min$ rate in the isotropic, nematic and ferroelectric nematic phases are shown in Figure 2. While in the N phase the texture is uniform, in

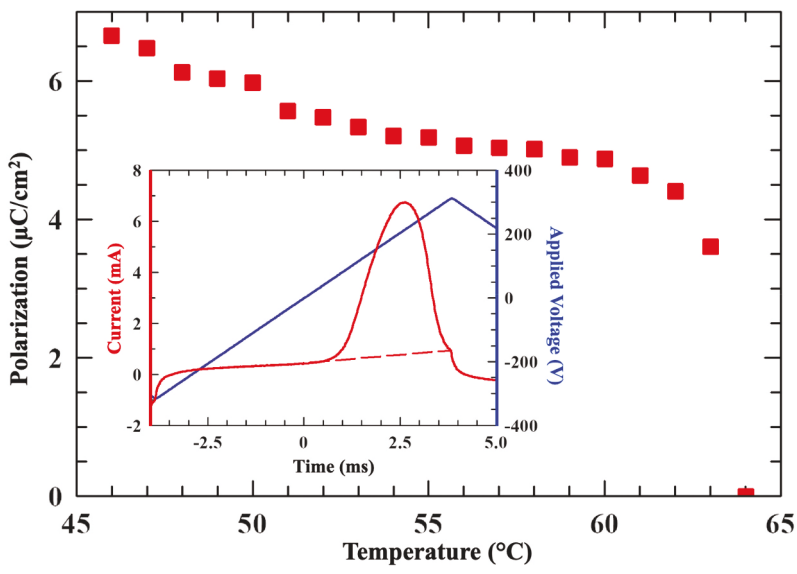

Figure 2. (Colour online) Temperature dependence of the spontaneous polarisation of RT11165. Inset: time dependence of the applied voltage plotted against the right axis and the measured current on the left axis at 58°C.

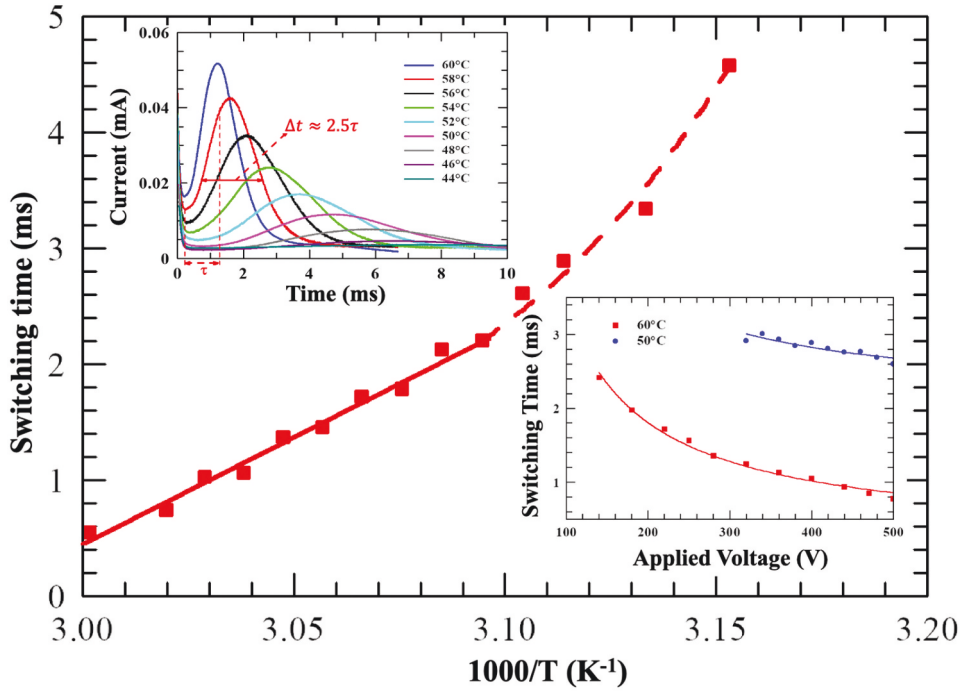

Figure 3. (Colour online) Summary of the switching time measurement of RT11165. Main panel: switching time versus $1000/T$, where T is the temperature in Kelvin scale. Solid red line shows the range corresponding to Arrhenius behavior, whereas the dotted red line is the fit using Vogel–Fulcher–Tammann (VFT) equation valid for viscous materials with a glass transition. Top-left inset: Time dependence of the electric current under 450 V, 40 Hz rectangular wave voltages applied across 0.5 mm gap between in-plane electrodes. Bottom-right inset: switching time versus applied voltage at 60°C and 50°C. Fits correspond to $\Delta t \propto U^{-1}$ function.

the N_F phase there are domains separated by defects with slightly different birefringence colors. These are due to coexistence of left and right-handed twisted domains related to the antiparallel rubbing of the substrates [30].

The temperature dependence of the spontaneous polarisation of RT11165 with an inset of the time dependence of the measured polarisation current and applied voltage, is shown in Figure 2. The polarisation could be measured only down to $46°C$ as at lower temperatures $U > 500V$ is required to fully switch the polarisation, so its value could be calculated from the area of the current curve above the dotted line shown in the inset to Figure 2. To obtain this, we not only had to increase the voltage, but also had to decrease the frequency, indicating that the viscosity of the material strongly increases on cooling. One can see that the polarisation increases from $P \approx 3.6\mu C/cm$ at $63°C$ to $P \approx 6.7\mu C/cm^2$ at $46°C$. The increase of the measured polarisation between $50°C$ and $46°C$ could be due to an increasing number of ions pushed through the electrodes at high voltages, or due to field-induced increase of the polar order parameter.

To measure the temperature dependence of the rotational viscosity of the material, we have measured the temperature and voltage dependences of the switching time, Δt determined as the full width at half maxima of the polarisation current peak as shown in the top left inset to Figure 3. It is found that the switching time is about 2.5 times larger than of the rise time τ. The switching time as a function of $1000/T$, where T is the temperature at Kelvin scale, is shown in the main panel of Figure 3. Between $1000/T \approx 3.0$ $(60°C)$ and $1000/T \approx 3.1(49°C)$ the dependence corresponds to an Arrhenius behavior $\Delta t = \Delta t_o \cdot e^{\frac{E_a}{k_B T}}$ with activation energy $E_a \approx 9\frac{kcal}{mol}$. Below about $46°C$ the dependence can be fitted only by the Vogel-Fulcher-Tammann (VFT) equation: $\Delta t = \Delta t_o \cdot e^{\frac{E_a}{k_B(T - T_{VFT})}}$, where k_B is the Boltzmann constant. The VFT equation is used to describe the viscosity (which is basically proportional to the switching time at constant field) of liquids in supercooled regime approaching the glass transition, where T_{VFT} typically is about 50°C below the glass transition temperature T_G. From the fit value of $T_{VFT} \approx 242K$ we deduce that the RT11165 becomes glassy at $T_G \sim 292K \sim 19°C$, i.e. close to room temperature.

As seen in the bottom-right inset to Figure 3, the applied voltage (U) dependence of the switching time is

found to be proportional to the inverse voltage ($\Delta t \propto U^{-1}$), which is expected from the relation between the switching time and the rotational viscosity γ_1 as $\Delta t \frac{\tilde{\gamma}_1}{P}$. From this, we can estimate the temperature dependence of the rotational viscosity by multiplying the temperature dependent switching time, the temperature dependent polarisation values (see Figure 2) and the applied field. We find that the rotational viscosity increases from about $30Pa.s$ at $57°C$ to $220Pa \cdot s$ at $41°C$.

To estimate the switching time and the rotational viscosity closer to the glass transition, we carried out electro-optical measurements at $25°C$ in a $d = 3.5\mu m$ thick antiparallel rubbed film with planar alignment by applying an $E = 0.2V/\mu m$ DC field between in-plane electrodes separated by $L = 0.5mm$ distance. At the instant the field is applied (0s, Figure 4(a)) the director is parallel to the rubbing direction (purple arrow) and the polarisation is opposite to the rubbing direction [31] making 45° with the crossed polarisers resulting in a light 1st order green color with optical path difference $\Delta n \cdot d \approx 770nm$. With $d = 3.5\mu m$ it indicates $\Delta n \approx 0.22$. After 15 seconds, the green birefringence color becomes darker, indicating the angle ϕ between the director and the electric field decreases due to rotation of the ferroelectric polarisation, as shown in Figure 4(b). After 24 seconds, the texture further darkens, indicating $\phi \sim 45°$, that is, the director is almost along one of the polariser axes. At the same time, the birefringence color changes from green to red corresponding to a decrease of the optical path difference to $\Delta n \cdot d \approx 550nm$. This indicates a tilt θ of the polarisation away from the in-plane direction (indicated by a white arrow with a nail) by $\theta \sim 40°$. After 35 seconds, the texture becomes brighter ($\phi < 45°$), and the dominating birefringence color becomes orange ($\Delta n \cdot d \sim 450\ nm$) indicating $\theta \sim 55°$ tilt. At 55s after field reversal, the texture becomes inhomogeneous with coexisting dark red and green colors showing inhomogeneous director structure. The red and green colors indicate $\theta \sim 40°$ and $\theta \sim 0°$ tilt, respectively. After 70s, the texture resembles the initial texture, showing that the director has rotated to parallel to the electric field ($\phi \sim 0°$) This shows that the switching time at $25°C$ is $\Delta t \sim 70s$, which assuming $P \sim 7 \cdot 10^{-2} C/m^2$ and with $E = 0.2V/\mu m$, gives $\gamma_1 \sim \Delta t \cdot P \cdot E \sim 10^6 Pa \cdot s$, i.e. 4 orders of magnitude larger than values above $40°C$. This, and the fact that we could not see any switching at $T \leq 20°C$, supports our previous suggestion of a glass transition at $T_G \sim 19°C$, where $\gamma_1 > 10^{13} Pa \cdot s$. While the rotation of the azimuthal angle ϕ is expected and agrees with previous electro-optical observations [15,16,30–34], the transient polar tilt away from the in-plane direction is unexpected. Although more studies are needed to explain this, we think it may be related to the viscoelastic nature of the director rotation due to the glass transition a few degrees below. Such a situation has been discussed previously [35] for

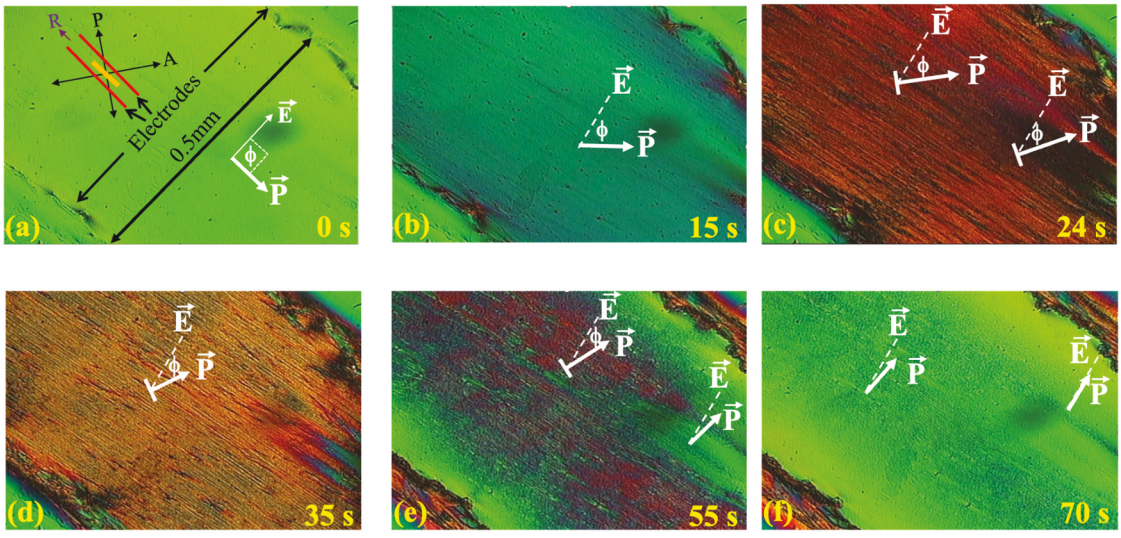

Figure 4. (Colour online) Electro-optical switching measurements of RT11165 at room temperature using DC voltage with rubbing direction parallel to the electrodes and perpendicular to the applied electric field. The cell is placed so that the electrodes are at 45° with respect to the polariser and analyser. At various time periods of the applied DC voltage: (a) 0 s, (b) 15 s, (c) 24 s, (d) 35 s, (e) 55 s and (f) 70 s. ϕ represents the direction of the in-plane polarisation with respect to the applied electric field. Nails at the end of the polarisation vector illustrate tilt away from the plane of the substrates.

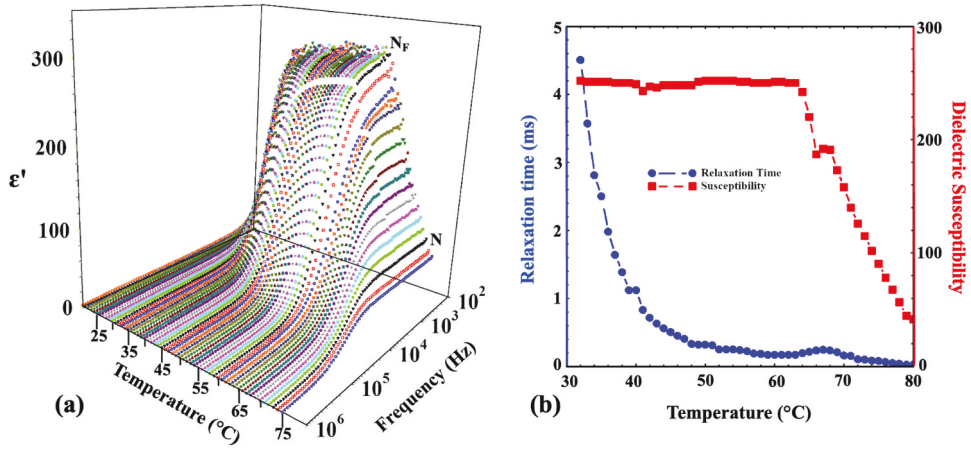

Figure 5. (Colour online) Summary of the dielectric measurements of RT11165 in a in 12.2 μm thick planar aligned sandwich cell using 45 nm thick rubbed PI2555 and 30 mV applied voltage. (a) 3D plot of ε' versus temperature between 22°C and 77°C and frequency between 100 Hz and 1 MHz. (b) Temperature dependence of the susceptibility and relaxation time between 30°C and 80°C.

a low molecular weight ferroelectric smectic liquid crystal.

To see how the glass transition affects the director relaxation time, we have carried out dielectric measurements in $d = 12.2\mu m$ thick planar aligned sandwich cell using $45nm$ thick rubbed PI2555 and $30mV$ applied voltage. The 3D plot (ε' versus temperature between $22°C$ and $77°C$, and frequency between $100Hz$ and $1MHz$) and the temperature dependences of the relaxation time and susceptibility are shown in Figure 5. The apparent dielectric constant increases almost linearly in the N phase from 48.8 at the $N-$ Itransition up to ~310 upon the transition to the N_F phase. On further cooling, it decreases slowly to about 300 at $45°C$, then it decreases strongly, reaching 37.9 at $22°C$. The temperature dependence of the susceptibility and relaxation time are shown in Figure 5(b) only above $30°C$, because at lower temperatures ε does not reach maximum above $100Hz$, therefore neither the susceptibility nor the relaxation frequency could be determined. Nevertheless, it can be seen that the relaxation time increases strongly below $45°C$, another sign of the glassy transition at lower temperatures. Note, the relaxation time (although it also shows critical increase on cooling) is orders of magnitude smaller than the switching time. This is because the relaxation time represents only small oscillations around the short axis of the director and not a full flipping as in case of the switching time. Another noteworthy observation is that the magnitude of the susceptibility that was determined from twice the height of the peak value of ε'', is slightly lower than the largest value of ε' (250 instead of $\sim$300), indicating an ionic contribution to ε' at low frequencies.

In addition, we have measured the parallel ($\varepsilon_{\|}$) and perpendicular ($\varepsilon_{\perp}$) components of the dielectric permittivity in the nematic phase at $1kHz$, $5kHz$ and $10kHz$ frequencies using $7\mu m$ cell with homeotropic and planar alignment coatings, respectively. The temperature dependence of the dielectric anisotropy ($\Delta\varepsilon = \varepsilon_{\|} - \varepsilon_{\perp}$) in the N phase is shown in Figure 6. The dielectric anisotropy is particularly elusive in the N_F phase, because homeotropic alignment is not achievable with standard surface treatments. These data demonstrate that the susceptibility to dielectric torque depends strongly both on the frequency and the distance from the N_F phase. Intriguingly, at higher ($5kHz$ and $10kHz$) frequencies the dielectric anisotropy exhibits a maximum at intermediate temperatures in the N phase. The behavior at $1kHz$ is similar to the temperature dependence of the susceptibility measured at the relaxation frequencies which drop below $1kHz$ in the N_F phase (see Figure 5(b)).

Finally, we note that recently Clark et al. [36] have argued that the measured large dielectric constant of the ferroelectric nematic liquid crystals is an artefact and what actually has been measured is not the capacitance of the liquid crystal, but of the non-ferroelectric, nanoscale interfacial insulating layer at the LC/electrode surface. This is due to the large polarisation P of the N_F material, which acts as conductor that charges up the insulating interfacial layer (called polarisation-capacitance-Goldstone (PCG) mode), resulting in an apparent static dielectric constant,

$$\varepsilon_A(0) = \varepsilon_I d/d_I, \tag{1}$$

where ε_I and d_I are the dielectric constant and thickness of the insulating layer and d is the thickness of the liquid crystal film. Furthermore, the characteristic relaxation time in the N_F phase was predicted as

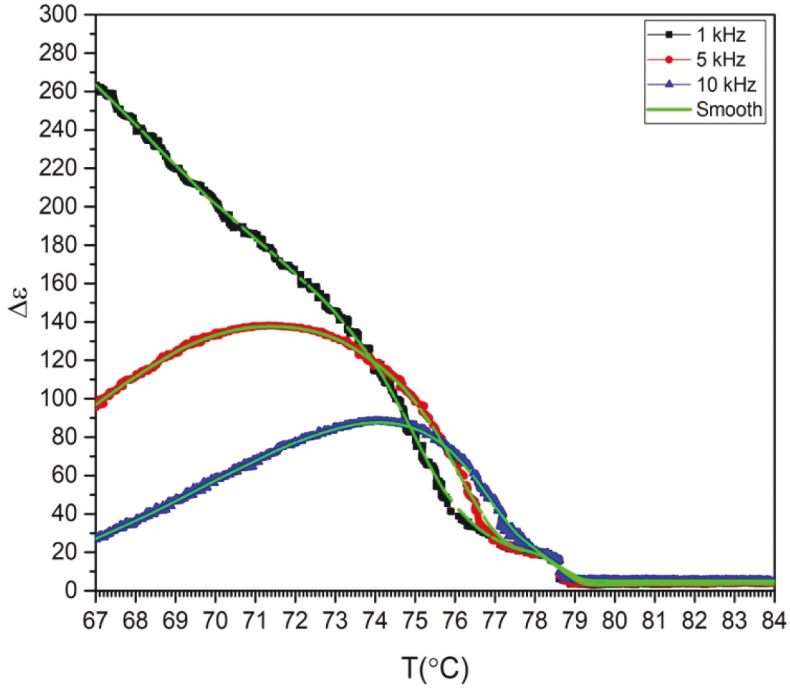

Figure 6. (Colour online) Temperature dependence of the dielectric anisotropy in the N phase at different frequencies.

$$\tau_o = \frac{\gamma_1 \varepsilon_I d}{P^2 d_I}, \tag{2}$$

where γ_1 is the rotational viscosity of the N_F director. In fact, very recently Erkoreka et al. [37] found that both the measured dielectric constant and the relaxation time are indeed proportional to the sample thickness, in accordance with the Clark et al. prediction. However, they argue that this could be also explained by the electrode polarisation (EP) effect, which is well-known for highly ionic fluids. Although we have not measured the dielectric spectra for different thicknesses, knowing all the parameters ($d = 12.2\mu m$, $d_I/2 = 45 \pm 5nm, and\ \varepsilon_I = 3.5 \cdot \varepsilon_o$ [38]) in the expression for the relaxation time derived by Clark et al., we can test the validity of Equations (1 and 2). For example, at 41°C, $P = 6.7 \cdot \frac{10^{-2}C}{m^2}; \gamma_1 = 220Pa \cdot s$ we would get for the relaxation time that $\tau_o \approx 0.43ms$. Within the measurement errors of γ_1 and d_I this agrees well with the measured $\tau_o \approx 0.7ms$ (see Figure 5(b)). Additionally, Equation (1) predicts that the apparent dielectric constant should be $\varepsilon_A(0) = 3.5 \cdot \frac{12200nm}{90nm} \sim 470$. This again represents a fairly good agreement with the measured $\varepsilon_A(100Hz) \sim 300$. The difference could be due to the fact that a measurement at 100 Hz does not accurately represent the static dielectric constant $\varepsilon_A(0Hz)$, as there is a further increase of ε_A below 100 Hz, as indeed seen in Figure 5(a).

4. Conclusions

In this paper we have described the synthesis, phase sequence and measurements of the temperature dependence of the ferroelectric polarisation and of rotational viscosity of a new ferroelectric nematic compound, 4-[(4-nitrophenoxy)carbonyl]phenyl 2-isopropoxy-4-methoxybenzoate (RT11165). We showed that although the molecular structure of RT11165 differs from the prototype ferroelectric nematic 4-[(4-nitrophenoxy)carbonyl]phenyl 2,4-dimethoxybenzoate (RM734) only by a substitution of the 2-methoxy group in the benzoic acid with a 2-isopropoxy group, there is a rather dramatic change in phase behaviour. While RM734 exhibits an N_F phase between 133°C and 90°C with a rotational viscosity well below $1Pa \cdot s$, the N_F phase in RT11165 extends from 63°C down to room temperature with rotational viscosity increasing to $10^6 Pa \cdot s$ at 23°C. This agrees with the temperature dependence of the switching time that indicates a glass transition at ~19°C. Analysis of our dielectric measurements combined with the material parameters seem to agree well with the polarisation-capacitance-Goldstone (PCG) mode of Clark et al. [36].

The glassy state found in RT11165 has also been observed in a number of related materials which differ in the exact identity of the 2-alkoxy group. Ferroelectric and piezoelectric glasses are promising materials for energy storage [39] and wastewater treatment by piezo catalysis [40]. The transparent and polar glassy state of

RT11165, which should be also piezoelectric [41], may therefore be a good candidate for these applications and potentially for data storage [42] as well.

Disclosure statement

No potential conflict of interest was reported by the author(s).

Funding

This work was financially supported by US National Science Foundation grant [DMR-2210083].

ORCID

P. Nepal http://orcid.org/0000-0002-3469-5459

References

[1] Bremer M, Kirsch P, Klasen-Memmer M, et al. The TV in your pocket: development of liquid-crystal materials for the new millennium. Angew Chem Int Ed. 2013;52:8880–8896. doi: 10.1002/anie.201300903
[2] Reinitzer F. Beiträge zur Kenntniss des Cholesterins. Monatshefte für Chemie und verwandte Teile anderer Wissenschaften. Monatshefte für Chemie – Chemical Monthly. 1888;9(1):421–441. doi: 10.1007/BF01516710
[3] Yu LJ, Saupe A. Observation of a biaxial nematic phase in potassium laurate-1-decanol-water mixtures. Phys Rev Lett. 1980;45(12):1000–1004. doi: 10.1103/PhysRevLett.45.1000
[4] Jákli A. Liquid crystals of the twenty-first century – nematic phase of bent-core molecules. Liq Cryst Rev. 2013;1:65–82. doi: 10.1080/21680396.2013.803701
[5] Dozov I. On the spontaneous symmetry breaking in the mesophases of achiral banana-shaped molecules. Europhys Lett. 2001;56(2):247–253. doi: 10.1209/epl/i2001-00513-x
[6] Cestari M, Diez-Berart S, Dunmur DA, et al. Phase behavior and properties of the liquid-crystal dimer 1′′,7′′-bis(4-cyanobiphenyl-4′-yl) heptane: a twist-bend nematic liquid crystal. Phys Rev E. 2011;84:031704. doi: 10.1103/PhysRevE.84.031704
[7] Jákli A, Lavrentovich OD, Selinger JV. Physics of liquid crystals of bent-shaped molecules. Rev Mod Phys. 2018;90:045004. doi: 10.1103/RevModPhys.90.045004
[8] Borshch V, Kim YK, Xiang J, et al. Nematic twist-bend phase with nanoscale modulation of molecular orientation. Nat Commun. 2013;4(1):4. doi: 10.1038/ncomms3635
[9] Chen D, Porada JH, Hooper JB, et al. Chiral heliconical ground state of nanoscale pitch in a nematic liquid crystal of achiral molecular dimers. Proc Natl Acad Sci USA. 2013;110:15931–15936. doi: 10.1073/pnas.1314654110
[10] Born M. Über anisotrope Flüssigkeiten. Versus einer Theorie der flüssigen Kristalle und des elektrischen Kerr-effekts in Füssigkeiten. Sitzungsber Preuss Akad Wiss. 1916;30:614–650.
[11] Nishikawa H, Shiroshita K, Higuchi H, et al. A fluid liquid-crystal material with highly polar order. Adv Mater. 2017;29(43):1702354. doi: 10.1002/adma.201702354
[12] Mandle RJ, Cowling SJ, Goodby JW. A nematic to nematic transformation exhibited by a rod-like liquid crystal. Phys Chem Chem Phys. 2017;19:11429–11435. doi: 10.1039/C7CP00456G
[13] Chen X, Korblova E, Dong D, et al. First-principles experimental demonstration of ferroelectricity in a thermotropic nematic liquid crystal: Polar domains and striking electro-optics. Proc Natl Acad Sci USA. 2020;117:14021–14031. doi: 10.1073/pnas.2002290117
[14] Sebastián N, Cmok L, Mandle RJ, et al. Ferroelectric-ferroelastic phase transition in a nematic liquid crystal. Phys Rev Lett. 2020;124:037801–1–6. doi: 10.1103/PhysRevLett.124.037801
[15] Sebastián N, Čopič M, Mertelj A. Ferroelectric nematic liquid crystalline phases. Phys Rev E. 2022;106:021001. doi: 10.1103/PhysRevE.106.021001
[16] Saha R, Nepal P, Feng C, et al. Multiple ferroelectric nematic phases of a highly polar liquid crystal compound. Liq Cryst. 2022;49:1784–1796. doi: 10.1080/02678292.2022.2069297
[17] Yu J-S, Lee JH, Lee J-Y, et al. Alignment properties of a ferroelectric nematic liquid crystal on the rubbed substrates. Soft Matter. 2023;2446:2446–2453. doi: 10.1039/D3SM00123G
[18] Long H, Li J, Huang M, et al. Mixing-induced phase stabilization and low-temperature-shifting of ferroelectric nematics. Liq Cryst. 2022;49:2121–2127. doi: 10.1080/02678292.2022.2104947
[19] Máthé MT, Perera K, Buka Á, et al. Fluid ferroelectric filaments. Adv Sci. 2023;202305950:1–8. doi: 10.1002/advs.202305950
[20] Gibb CJ, Hobbs JL, Nikolova DI, et al. Spontaneous symmetry breaking in polar fluids. ArXiv. 2024:0207305.
[21] Manabe A, Bremer M, Kraska M. Ferroelectric nematic phase at and below room temperature. Liq Cryst. 2021;48:1079–1086. doi: 10.1080/02678292.2021.1921867
[22] Mandle RJ. In silico interactome of a room-temperature ferroelectric nematic material. Crystals (Basel). 2023;13(6):857. doi: 10.3390/cryst13060857
[23] Parton-Barr C, Gleeson HF, Mandle RJ. Room-temperature ferroelectric nematic liquid crystal showing a large and divergent density. Soft Matter. 2023;20:672–680. doi: 10.1039/D3SM01282D
[24] Mandle RJ, Cowling SJ, Goodby JW. Rational design of rod-like liquid crystals exhibiting two nematic phases. Chem A Euro J. 2017;23:14554–14562. doi: 10.1002/chem.201702742
[25] Pociecha D, Walker R, Cruickshank E, et al. Intrinsically chiral ferronematic liquid crystals: an inversion of the helical twist sense at the chiral nematic – chiral ferronematic phase transition. J Mol Liq. 2022;361:361. doi: 10.1016/j.molliq.2022.119532
[26] Cruickshank E, Walker R, Storey JMD, et al. The effect of a lateral alkyloxy chain on the ferroelectric nematic phase. RSC Adv. 2022;12(45):29482–29490. doi: 10.1039/D2RA05628C

[27] Tufaha N, Cruickshank E, Pociecha D, et al. Molecular shape, electronic factors, and the ferroelectric nematic phase: investigating the impact of structural modifications. Chem A Euro J. 2023;29:e202300073. doi: 10.1002/chem.202300073
[28] Lundquist PM, Wortmann R, Geletneky C, et al. Organic glasses: a new class of photorefractive materials. Science. 1996;274:1182–1185. doi: 10.1126/science.274.5290.1182
[29] Zhao X, Zhou J, Li J, et al. Spontaneous helielectric nematic liquid crystals: electric analog to helimagnets. Proc Natl Acad Sci USA. 2021;118:e2111101118. doi: 10.1073/pnas.2111101118
[30] Chen X, Korblova E, Glaser MA, et al. Polar in-plane surface orientation of a ferroelectric nematic liquid crystal: polar monodomains and twisted state electro-optics. PNAS. 2021;118:e2104092118. doi: 10.1073/pnas.2104092118
[31] Basnet B, Rajabi M, Wang H, et al. Soliton walls paired by polar surface interactions in a ferroelectric nematic liquid crystal. Nat Commun. 2022;13(1):s41467s41467–31593–w. doi: 10.1038/s41467-022-31593-w
[32] Hsiao YT, Nys I, Neyts K. Lateral electric field switching in thin ferroelectric nematic liquid crystal cells. Soft Matter. 2023;19(44):8617–8624. doi: 10.1039/D3SM00997A
[33] Sebastián N, Mandle RJ, Petelin A, et al. Electrooptics of mm-scale polar domains in the ferroelectric nematic phase. Liq Cryst. 2021;48:2055–2071. doi: 10.1080/02678292.2021.1955417
[34] Caimi F, Nava G, Fuschetto S, et al. Fluid superscreening and polarization following in confined ferroelectric nematics. Nat Phys. 2023;19(11):1658–1666. doi: 10.1038/s41567-023-02150-z
[35] Jákli A, Saupe A. Viscoelastic director rotation of a low molecular mass liquid crystal. Liq Cryst. 2001;28:827–831. doi: 10.1080/02678290110034511
[36] Clark NA, Chen X, Maclennan JE, et al. Dielectric spectroscopy of ferroelectric nematic liquid crystals: measuring the capacitance of insulating interfacial layers. Phys Rev Research. 2024;6:013195. doi: 10.1103/PhysRevResearch.6.013195
[37] Erkoreka A, Martinez-Perdiguero J, Mandle RJ, et al. Dielectric spectroscopy of a ferroelectric nematic liquid crystal and the effect of the sample thickness. J Mol Liq. 2023;387:122566–1–8. doi: 10.1016/j.molliq.2023.122566
[38] Lin AW. Evaluation of polyimides as dielectric materials for multichip packages with multilevel interconnection structure. IEEE Trans Comp Hybrids Manufact Technol. 1990;13:207–213. doi: 10.1109/33.52872
[39] Khalf AZ. Ferroelectric Glass-Ceramic Systems for Energy Storage Applications. Adv Ceram Mater. 2020.
[40] Singh G, Sharma M, Vaish R. Transparent ferroelectric glass–ceramics for wastewater treatment by piezocatalysis. Commun Mater. 2020;1(1):1–8. doi: 10.1038/s43246-020-00101-2
[41] Máthé MT, Himel MSH, Adaka A, et al. Liquid piezoelectric materials: linear electromechanical effect in fluid ferroelectric nematic liquid crystals. Adv Funct Mater. 2024;2314158:1–7. doi: 10.1002/adfm.202314158
[42] Rauch S, Selbmann C, Bault P, et al. Glass forming banana-shaped compounds: vitrified liquid crystal states. Phys Rev E. 2004;69:021707–7. doi: 10.1103/PhysRevE.69.021707